Review Article
cnj.araku.ac.ir

☑ Cite This: Colloid Nanosci. J. 3(4) (2025) 753-767 DOI: 10.61882/CNJ.3.4.753

Green-Synthesized Zinc Ferrite Nanoparticles as Efficient Catalysts for the Synthesis of Oxazolone and Thiazolidinedione Derivatives

Akbar Mobinikhaledi[1]*, Hassan Moghanian[2], Najmieh Ahadi[1], Yousef Mansoori[1]

[1]Department of Chemistry, Faculty of Science, Arak University, Arak, Iran
[2]Department of Chemistry, Dez.C., Islamic Azad University, Dezful, Iran

ARTICLE INFO

Article History:
Received 2025-11-30
Revised 2026-02-01
Accepted 2026-02-06
Published 2026-02-06

Corresponding Authors:
Akbar Mobinikhaledi
Email:
akbar_mobini@yahoo.com

ABSTRACT

This work addresses the research gap in the use of environmentally friendly zinc ferrite nanocatalysts and plant-based intermediates for efficient synthesis of heterocyles, while combining innovation, environmental rationale, and practical applications. For this purpose, $ZnFe_2O_4$ functionalized with thioglycolic acid ($ZnFe_2O_4$-TGA) nanoparticles were synthesized through a stepwise functionalization and coupling process, resulting in a multipurpose material with improved biocompatible properties. Various analytical techniques including Fourier-transform infrared spectroscopy (FT-IR), X-ray diffraction (XRD), field emission-scanning electron microscope (FE-SEM), Energy dispersive X-ray analyzer (EDX), TEM, Vibrating sample magnetometry (VSM), and Thermogravimetric (TGA), were used to analyze the structure of these magnetic nanoparticles. The application of these nanoparticles as a catalyst in the synthesis of oxazolone and thiazolidinedione derivatives were investigated. The findings highlight the potential of $ZnFeO_4$–TGA nanoparticles as efficient, green, and recyclable catalysts for the synthesis of oxazolone and thiazolidinedione derivatives with desirable yields.

KEYWORDS: *Green synthesis; Azlactone; Thiazolidinedione; Zinc ferrite; Magnetic nanoparticles*

1. Introduction

Green chemistry plays a crucial role in modern research by promoting environmentally benign chemical processes, particularly through the use of efficient and recyclable catalysts. In this context, heterogeneous nanocatalysts, especially magnetic nanoparticles, have attracted significant attention due to their sustainability and ease of separation [1, 2].

Transition metal ferrites with the general formula MFe_2O_4 (M = Cu, Zn, Ni, etc.) exhibit remarkable physicochemical properties and have found widespread applications in catalysis, biomedicine, environmental remediation, and energy-related processes [3-5]. Among them, zinc ferrite nanoparticles are of particular interest due to their chemical stability and tunable functional properties. When these magnetic nanoparticles are used as catalyst supports, they enable rapid recovery via an external magnetic field, increasing catalytic efficiency and recyclability [6-8].

Recently, plant-mediated green synthesis has emerged as an eco-friendly, cost-effective, and one-pot strategy for preparing nanoparticles. Plant extracts rich in bioactive compounds such as polyphenols and flavonoids, can act simultaneously as reducing and stabilizing agents, eliminating the need for toxic chemicals [9-11]. In this study, walnut (Juglans regia) leaf extract was selected as a renewable and underutilized natural resource, offering a sustainable route for the synthesis of magnetic nanocatalysts [12, 13].

Oxazolones (azlactones), particularly 4-arylidene-2-phenyl-5(4H)-oxazolones,

are important heterocyclic compounds with notable biological and pharmaceutical activities, including anticancer and anti-HIV properties [14-17]. Although numerous synthetic methods using different catalysts and reagents have been developed for synthesis of oxazolones [18, 19], some of them suffer from limitations such as harsh conditions, toxic solvents, long reaction times, and low yields. Therefore, the development of greener and more efficient catalytic systems for synthesis of these compounds remains highly desirable.

Similarly, thiazolidin-4-ones constitute an important class of biologically active heterocycles that exhibit a wide range of pharmacological activities such as antimicrobial, anti-inflammatory, anti-tuberculosis, and anticancer effects [20-22]. Considerable efforts have focused on the three-component synthesis of 2,3-diarylthiazolidin-4-ones using various acid catalysts; however, challenges related to sustainability and operational simplicity persist [23, 24].

The present study focuses on the green synthesis of MFe_2O_4 and MFe_2O_4-TGA nanocomposites using walnut leaf extract and investigates their catalytic performance in the preparation of oxazolone and thiazolidinedione derivatives under mild, sustainable, and recyclable conditions.

2. Experimental

2.1. Materials and methods

The used chemical reagents were purchased from Fluka, Merck and Aldrich chemical companies and used without further purification. The FT-IR spectra were recorded by Brucker alpha series in the rage of 400-4000 cm^{-1} (using KBr pellets). Surface morphological was performed by Field Emissive Scanning Electron Microscopy (FE-SEM, Philips FEI Quanta-200f) and Energy Dispersive X-ray Analysis (EDAX, Oxford Instruments). The crystalline structure of the samples was investigated at room temperature by X-ray powder diffractometric Bruker AX500 X-ray diffractometer under Cu-Kα radiation (0.154 nm). The magnetic behavior of samples was examined using a Vibrating Sample Magnetometer (VSM) (Lakeshore-Model: 7404) at room temperature. ^1H and ^{13}C NMR spectra were obtained by Brucker Avence spectrometer at 300 and 75 MHz, respectively, using DMSO-d_6 as a solvent. Thermogravimetric analysis (TGA) was performed by TA instruments Q 5000 system to characterize the thermal stability of the catalyst in the temperature range of 30 to 700 °C with a heating rate of 10 °C/min under nitrogen atmosphere.

2.2. Preparation of $ZnFe_2O_4$ nanoparticles

In a 250 mL three-necked flask equipped with a magnetic stirrer, 75 mL of distilled water and 25 mL of ethanol were poured. Subsequently, 10 g of dried walnut leaves were crushed and transferred to the flask. The mixture was refluxed for four hours to obtain the extract, then filtered through filter paper to remove any remaining solids. Two different solutions were prepared. Solution A: In a 250 mL flask, 50 mL of walnut leaf extract, 40 mL of n-hexane, 20 mmol of iron (III) chloride, and 10 mmol of zinc acetate were added. The addition of n-hexane creates a biphasic environment that improves the dispersion of metal ions, facilitates controlled nucleation, and helps achieve uniform nanoparticle morphology. Solution B: A solution of 90 mmol of ammonium carbonate dissolved in 50 mL of walnut leaf extract. Solution B was transferred into a separatory funnel, allowing it to be slowly added dropwise to Solution A, while solution A was being stirred using a magnetic stirrer. The obtained precipitate was filtered through filter paper, thoroughly washed with deionized water, and dried. Subsequently, the material was calcined in an electric furnace at 600 °C for 2 hours, resulting in the formation of $ZnFe_2O_4$ nanoparticles.

2.3. Preparation of $ZnFe_2O_4$-TGA nanoparticles

2 g of the prepared $ZnFe_2O_4$ nanoparticles were transferred to a 100 mL flask containing 10 mL of THF and 2 mmol of thioglycolic acid. The mixture was sonicated for 30 minutes. Finally, the resulting precipitate was filtered, washed, and dried, yielding the prepared $ZnFe_2O_4$-TGA nanocatalyst.

2.4. General procedure for the azlactone derivatives synthesis catalysed by $ZnFe_2O_4$ nanocatalyst

In an experimental tube, a mixture of aldehyde (**1**) (1 mmol), hippuric acid (**2**) (1 mmol), acetic anhydride (0.5 g), and $ZnFe_2O_4$ nanoparticles (20 mg) was subjected to microwave irradiation. The reaction was performed using a National Microwave Oven, Model No. NN-K571MF (2450 MHz, 450 W) for 1-2 minutes. The progress of the reaction was monitored by TLC. Upon completion of the reaction, the reaction mixture was dissolved in a minimal amount of hot ethanol. After filtration, the catalyst was separated. The resulting clear solution

was allowed to stand at room temperature for 2 hours before being concentrated. The obtained precipitate (**3**) was filtered, washed, and dried.

2.5. General procedure for the synthesis 4-thiazolidinone derivatives catalysed by $ZnFe_2O_4$-TGA nanocatalyst

In a test tube, a mixture of desired aldehyde (**4**) (1 mmol), amines (**5**) (1 mmol), thioglycolic acid (**6**) (1.5 mmol), and the $ZnFe_2O_4$-TGA nanocatalyst (30 mg) was stirred using a magnetic stirrer under solvent-free conditions and heated at 80 ºC using a thermostatically controlled oil bath, ensuring a stable reaction temperature. The reaction progress was monitored using TLC. After the reaction was complete, as detected by TLC, the reaction mixture was cooled to form the desired crystals (**7**). The crystals were separated with a funnel and filter paper and then purified by repeated washing with ethanol and water.

2.6. Selected spectra data

4-(4-chlorobenzylidene)-2-phenyloxazol-5(4H)-one (3d)

IR (KBr): ν_{max} = 3092, 1796, 1655, 1589, 1555, 1487, 1410, 1325, 1300, 1161, 1094, 984, 866, 826, 777, 694, 556, 488, 397 cm^{-1}; ^1H NMR (300 MHz, $CDCl_3$): δ= 8.2(d, J=8.4 Hz, 2H), 8.17(d, J= 8.4 Hz, 2H), 7.65(t, J=7.4 Hz, 1H), 7.56(t, J=7.5 Hz, 2H), 7.47(d, J=8.7 Hz, 2H), 7.21(s, 1H) ppm. ^{13}C NMR (75 MHz, $CDCl_3$): δ= 167.3, 163.8, 137.2, 133.6, 133.56, 133.52, 132.0, 130.0, 129.2, 129.0, 128.4, 125.4 ppm.

2-phenyl-4-(thiophen-2-ylmethylene) oxazol-5(4H)-one (3h)

IR(KBr): ν_{max} = 3091, 790, 1647, 1555, 1460, 1327, 1298, 1153, 1053, 982, 856,799, 698, 534, 492 cm^{-1}. ^1H NMR (300 MHz, $CDCl_3$): δ= 8.19(d, J= 7.8 Hz, 2H), 7.75(d, J= 7.8 Hz, 1H), 7.64-7.54(m, 4H), 7.5(s, 1H), 7.19(dd, J= 4.2, 4.5 Hz, 1H) ppm. ^{13}C NMR (75 MHz, $CDCl_3$): 166.9, 162.4, 137.6, 135.3, 134.9, 133.1, 130.9, 128.9, 128.3, 127.9, 125.6, 124.8 ppm.

2-phenyl-3-(p-tolyl) thiazolidin-4-one (7a)

IR(KBr): ν_{max}= 2914, 1669, 1513, 1415, 1245, 1089, 815, 670 cm^{-1}. ^1H NMR(300 MHz, DMSO-d_6): 7.30 (1H, t, J= 7.4 Hz),7.29(2H, d, J= 7.4 Hz), 7.27(2H, t, J= 7.4 Hz), 7.14(2H, d, J= 8.4 Hz), 7.12(2H, d, J= 8.4 Hz), 6.06(1H, d, J = 1.5), 4.03(1H, dd, J = 15.8, 1.5 Hz), 3.90(1H, d, J= 15.8 Hz), 2.21(3H, s) ppm. ^{13}C NMR (75 MHz, DMSO-d_6): 21.3, 33.5, 72.6, 120.2, 126.9, 128.6, 129.2, 133.4, 138.2, 139.2,142.8, 174.2 ppm.

3-(4-bromophenyl)-2-(3-nitrophenyl) thiazolidin-4-one (7e)

IR (KBr): ν_{max}= 3067, 2966, 1687, 1530, 1391, 1350, 1219, 903, 829, 807, 725. ^1H NMR(300 MHz, DMSO-d_6): 8.25(1H, s),8.1(1H, d, J = 7.4), 7.9(2H, t, J= 7.4), 7.6(2H, d, J = 8.4), 7.5(1H, d, J = 8.4), 7.33 (1H, t, J= 1.5), 6.7(1H, s), 3.90(2H, dd, J= 15.8) ppm. ^{13}C NMR (75 MHz, DMSO-d_6): 33.13, 40.2, 62.46, 119.7, 122.3, 127.2, 130.4, 132.2, 134.20, 136.9, 142, 148.2, 170.9 ppm.

3. Results and discussion

3.1. Characterization of $ZnFe_2O_4$-TGA nanocatalyst

Thioglycolic acid-functionalized zinc ferrite nanoparticles were synthesized following the procedure outlined in Scheme 1. Fourier transform infrared (FT-IR) spectroscopy, field emission scanning electron microscopy (FE-SEM), energy dispersive X-ray spectroscopy (EDS), X-ray diffraction (XRD), thermogravimetric analysis (TGA) and vibrating sample magnetometry (VSM) were employed to identify and characterize the eco-friendly, gentle, and innovative magnetic catalyst.

Figure 1a displays typical Fourier-Transform Infrared (FTIR) spectra of $ZnFe_2O_4$ calcined at 600 °C. The spectra confirm the formation of the ferrite phase, characterized by two distinct absorption bands corresponding to intrinsic metal-oxygen stretching vibrations at tetrahedral (A) and octahedral (B) sites, a hallmark of spinel ferrites [25]. The higher wavenumber band (ν1) signifies the intrinsic stretching vibration of metal-oxygen at a sites, while the lower wavenumber band (ν2) indicates the intrinsic stretching vibrations at B sites. The FTIR analysis reveals that ν2 falls within the range of 420 cm^{-1} and ν1 within the range of 540 cm^{-1}. In curve 1b, the spectrum of $ZnFe_2O_4$-TGA nanoparticles reveals absorptions around 420 and 540 cm^{-1}, corresponding to the bending vibration of Zn-O and Fe-O bonds. Additionally, an absorption band appears at 1711 cm^{-1}, indicating the presence of the C=O group and confirming the functionalization of zinc ferrite nanoparticles with thioglycolic acid (Table 1).

Figure 2 presents the X-ray diffraction (XRD)

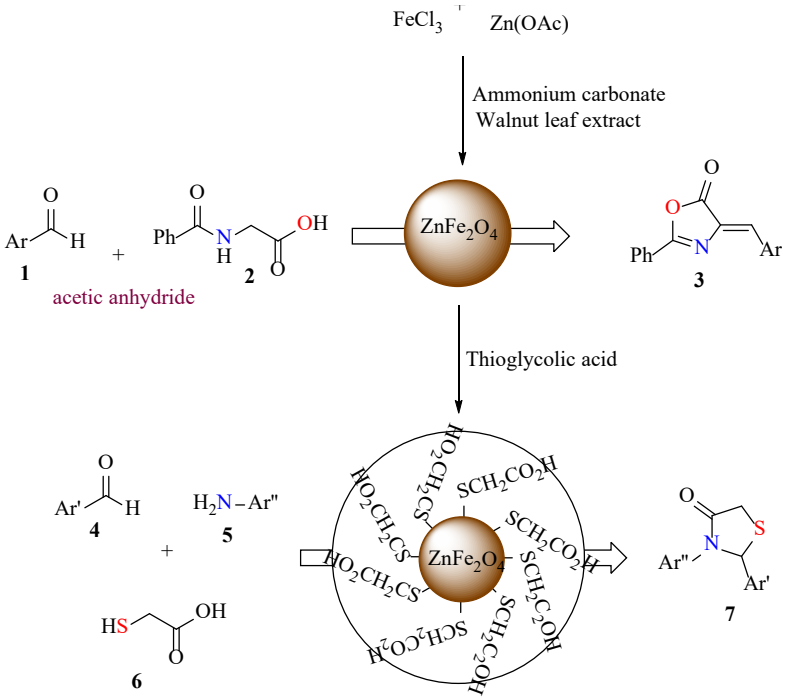

Scheme 1. Synthesis of zinc ferrite ($ZnFe_2O_4$) and thioglycolic acid-functionalized zinc ferrite ($ZnFe_2O_4$-TGA) nanoparticles and synthesis of azlactone and 4-thiazolidinone derivatives using these nanomaterials.

Table 1. The comparison of FT-IR spectra of ZnFe2O4 and ZnFe2O4-TGA.

composite	Fe-O ν (cm^{-1})	Zn-O ν (cm^{-1})	C=O ν (cm^{-1})
$ZnFe_2O_4$	540	420	-
$ZnFe_2O_4$-TGA	538	418	1711

pattern of $ZnFe_2O_4$ nanoparticles, captured at room temperature within a 2θ range of 20° to 80° using Cu Kα radiation (λ = 1.5406 Å). All observed peaks align with the expected reflections of the cubic $ZnFe_2O_4$ phase, consistent with the standard JCPDS card no. 01-089-101 [26]. Specifically, peaks at 2θ values of 30.06°, 35.41°, 43.04°, 53.51°, 57.00°, and 62.57° confirm the cubic $ZnFe_2O_4$ phase. Notably, no peaks indicative of ZnO or Fe_2O_3 were detected, signifying the formation of pure $ZnFe_2O_4$ [27].

The lattice parameter of the synthesized $ZnFe_2O_4$ nanoparticles was calculated from the XRD data using the Bragg equation and the cubic spinel relation $a = d\sqrt{h^2 + k^2 + l^2}$. The diffraction peaks corresponding to the (220), (311), (400), (422), (511), and (440) planes were used for calculation. The obtained lattice parameter values are ranged from 8.34 to 8.41 Å, with an average value of 8.38 Å, which is in good agreement with the reported lattice parameter of cubic $ZnFe_2O_4$, confirming the formation of a pure spinel structure.

The average crystallite size was calculated using the Scherrer equation: $D = 0.9\lambda/\beta \cos\theta$, where λ represents the X-ray wavelength, β is the full width at half maximum (FWHM) of the diffraction line in radians, θ is the Bragg diffraction angle, and D is the average diameter in Å. The peak at 2θ = 35.41° was used for this calculation. Based on the equation, the estimated diameter of $ZnFe_2O_4$ and $ZnFe_2O_4$-TGA nanoparticles was approximately 25 nm, 29 nm, respectively. Furthermore, comparison of the XRD patterns revealed that the modified nanoparticles retained their crystalline structure throughout the modification process.

FE-SEM, histogram chart and energy dispersive X-ray spectroscopy (EDS) are presented in Figure 3. FE-SEM was employed to analyze the size and morphology of the prepared $ZnFe_2O_4$ and $ZnFe_2O_4$-TGA catalysts (Fig. 3a, b). $ZnFe_2O_4$ particles, depicted in Figure 3(a), exhibit a mean diameter of approximately 20-30 nm, while in Fig. 3b, $ZnFe_2O_4$-TGA particles show a mean diameter of about 35 nm. Both types of particles exhibit a near-spherical morphology, which implies a large surface area for the nanocatalyst. It is clear that the organic compounds in the extract may have covered or stabilized the nanoparticles during their formation; as a result, the particles are smaller, well dispersed, and almost uniform in appearance. Although ammonium carbonate acts as a precipitating agent,

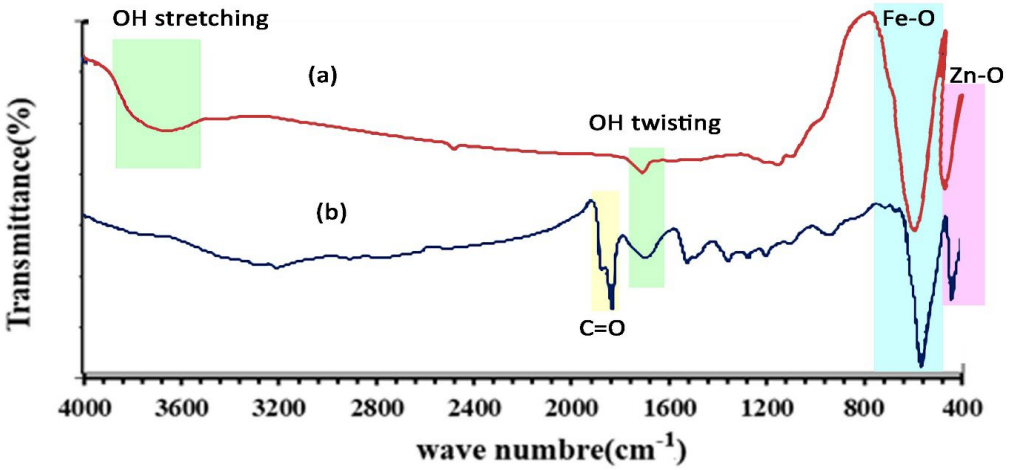

Fig. 1. FTIR spectra of (a) ZnFe2O4 and (b) ZnFe2O4-TGA nanoparticles.

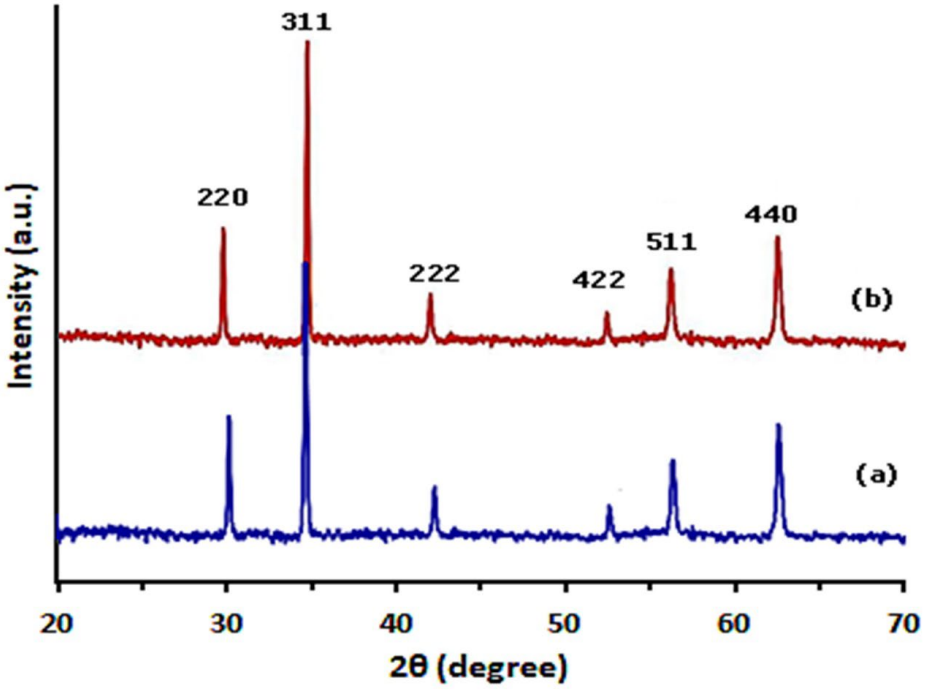

Fig. 2. XRD patterns of (a) ZnFe2O4 and (b) ZnFe2O4-TGA nanoparticles.

it is noteworthy that the effects of the extract and the precipitating action both have an effect on the formation of nanoparticles with smaller sizes.

The Histogram chart of (c) $ZnFe_2O_4$ showed a distribution of nanoparticle size between 18-20 nm, while $ZnFe_2O_4$-TGA showed a distribution of size between 20-30 nm. The findings are consistent with the results of FE-SEM analyses.

The results of energy dispersive X-ray spectroscopy (EDS) (Figure 4) from a single CNC revealed that it was primarily composed of Zn, Fe, and O, with no other elemental impurities present in the zinc ferrite nanoparticles (Fig. 3b). The presence of S, C, O, Fe, and Zn atoms are confirmation of the $ZnFe_2O_4$-TGA (Fig.3d) construction nanoparticles and the presence of S and C signals confirms that thioglycolic acid molecules are loaded on $ZnFe_2O_4$. The reported elemental percentages are semiquantitative estimates based on relative peak intensities of EDX spectra and do not show actual weights or atomic weight percentages.

Figure 5 depicts the thermogravimetric analysis (TGA) and differential thermogravimetric analysis (DTG) curves of $ZnFe_2O_4$-TGA nanoparticles. An initial weight loss, reaching approximately 120°C, is attributed to the removal of physically adsorbed solvent molecules and surface hydroxyl groups. Beyond this temperature, a substantial weight loss (roughly 120 °C to 520 °C) is observed, which can be ascribed to the decomposition of the organic layer present in the nanocatalyst. This behavior suggests reasonable stability of the catalyst up to 300°C, rendering it suitable for heterogeneous reactions. Notably, this weight loss step implies an organic material loading of approximately 33 wt.% on the magnetic catalyst, supported by thioglycolic acid on $ZnFe_2O_4$ MNPs. For comparison, $ZnFe_2O_4$ NPs exhibited a weight loss of 5.5 wt.%, likely due to the removal of excess water [28]. Also, the DTG analysis showed a good thermal stability up 170 °C for $ZnFe_2O_4$-TGA nanoparticles.

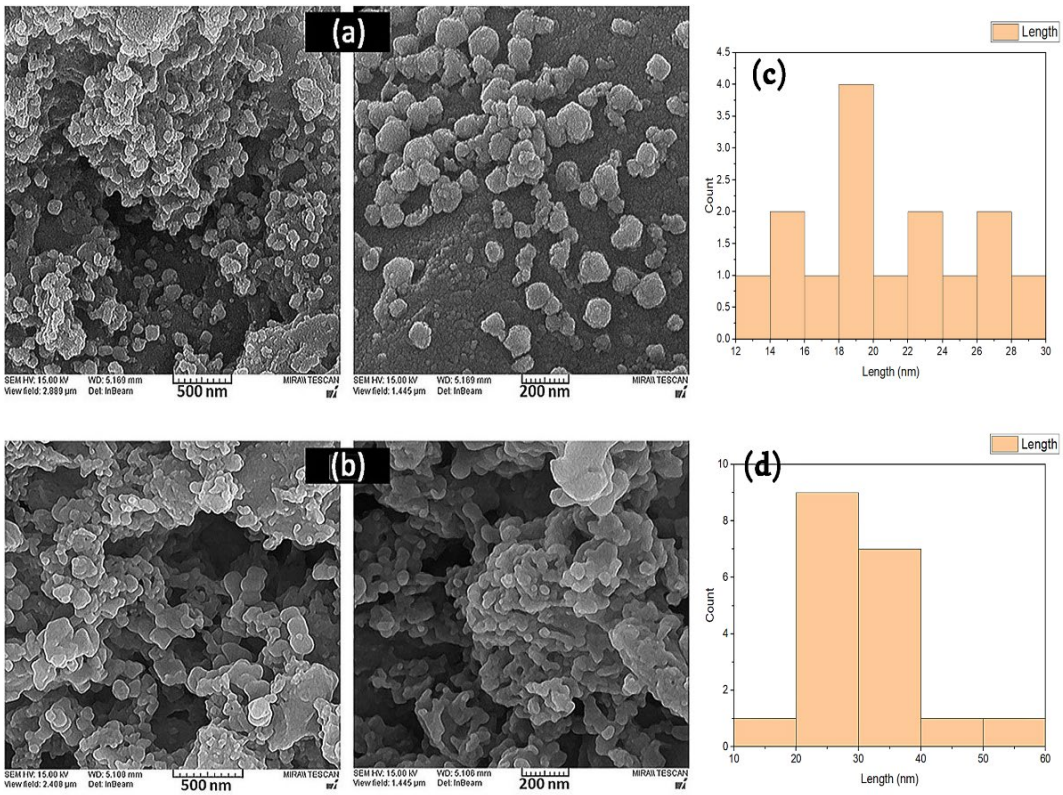

Fig. 3. FE-SEM images (a) ZnFe2O4 and (b) ZnFe2O4-TGA nanoparticles, histogram chart (c) ZnFe2O4 and (d) ZnFe2O4-TGA).

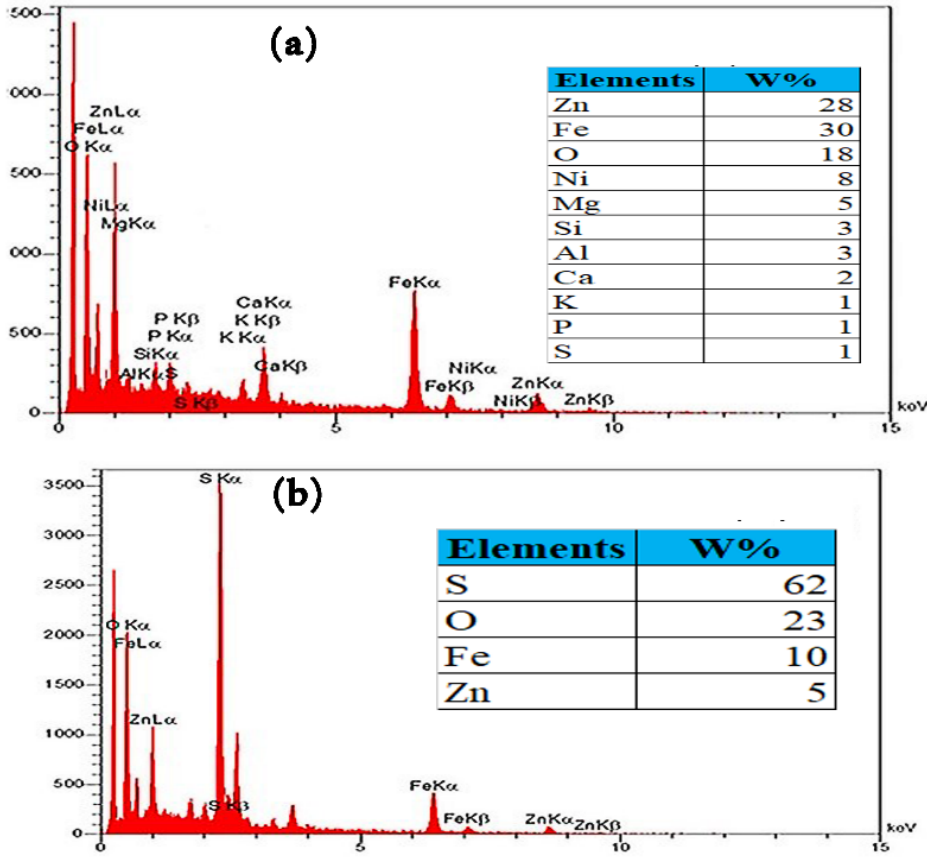

Fig. 4. EDX analyses of ZnFe2O4 (e) and (f) ZnFe2O4-TGA nanoparticles.

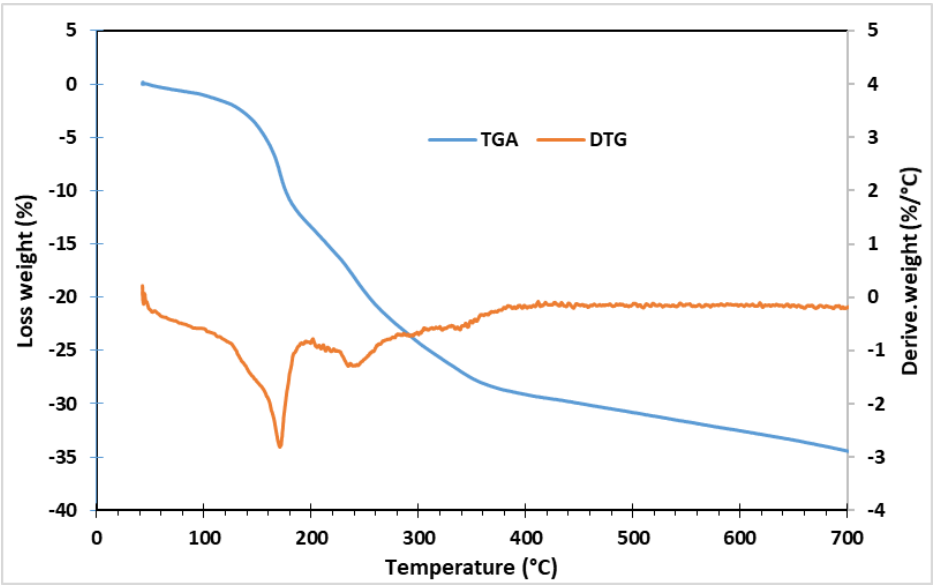

Fig. 5. TGA curves of ZnFe2O4-TGA nanoparticles.

Figure 6 displays the room-temperature magnetization curves of bare $ZnFe_2O_4$ (a) and $ZnFe_2O_4$-TGA (b) nanoparticles, measured using a vibrating sample magnetometer (VSM). The hysteresis loops allow for the extraction of key magnetic parameters like coercivity (Hc), remanent magnetization (Mr), and saturation magnetization (Ms). Notably, both samples reached full magnetization saturation under high fields (up to ±8500 Oe). However, the organic layer coating the $ZnFe_2O_4$ core in $ZnFe_2O_4$-TGA resulted in a variation in Ms Values, ranging from 33 to 15 emu g^{-1}. Table 2 indicates a comparison of magnetization curves of bare $ZnFe_2O_4$ in the present study and other reported works. Entry 1 presents the VSM analysis of uncoated $ZnFe_2O_4$ nanoparticles synthesized via a simple route using zinc(II) nitrate, iron(III) nitrate, and lactose, as reported by Bigleri *et al.* [29]. Entries 2 and 3 are $ZnFe_2O_4$ nanoparticles prepared via the co-precipitation method [30, 31]. This comparison shows that $ZnFe_2O_4$-TGA nanoparticles offer suitable magnetic properties.

3.2. Synthesis of oxazolone and thiazolidinedione derivatives

Following the characterization of the prepared $ZnFe_2O_4$ nanoparticles, their catalytic activity was evaluated in the synthesis of oxazolone derivatives, using nanomaterials synthesized from walnut leaf extract. To determine the optimal reaction conditions, the reaction of benzaldehyde (1 mmol), hippuric acid (1 mmol), and acetic anhydride (0.5 g) was selected for synthesis of 3a as a model and investigated under various conditions. Several solvents including acetonitrile, chloroform,

Table 2. The comparison of magnetization curves of bare ZnFe2O4

Entry	saturation magnetization (emu/g)	Reference
1	0.9	[29]
2	20	[30]
3	16.51	[31]
4	33	This work

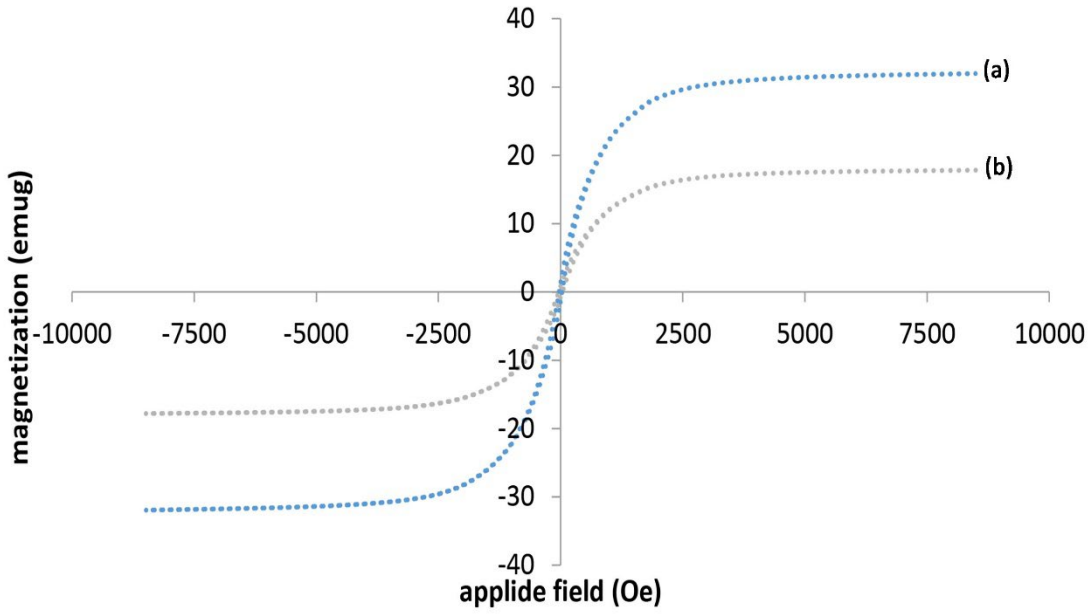

Fig. 6. Magnetic hysteresis loops of ZnFe2O4 and ZnFe2O4-TGA.

1,4-dioxane, ethyl acetate, and tetrahydrofuran, along with solvent-free and microwave conditions were explored. As the results, show (Table 3, no product was obtained when using THF and $CHCl_3$ solvents (Table 3, entry 1 and 4) while in 1,4-dioxane, ethyl acetate and acetonitrile solvents product was observed in low yield (Table 3, entry 3, 2, etc.)

The solvent-free conditions at room temperature offered low product yield (Table 3, entry 6). With the increase in temperature, the rate of product formation also increased, which can be due to providing the activation energy for the reaction and finally leads to the formation of oxazolone (Table 3, entry 7 and 8). No product was obtained at high temperature and in the absence of catalyst (Table 3, entry 9). However, under solvent-free and microwave conditions in the presence of catalyst, a product with a high yield (98%) was obtained (Table 3, entry 10).

In the next step, as can see in Table 1 (entry 10-14), choosing the best amount for the catalyst and the best time for the reaction were investigated. Therefore, solvent-free conditions, 50% microwave power (450W) and 20 mg catalyst were found optimal conditions for this reaction.

In order to study the capabilities and limitations of this method, a series of experiments were conducted using different aromatic aldehydes (Table 4). Aromatic aldehydes, which contained electron-withdrawing and less sterically hinder groups, showed better reactivity and promoted the reactions with greater yield of the products.

A suggested mechanism for the reaction of aromatic aldehydes and hippuric acid in the presence of zinc ferrite nanoparticles for the preparation of their 2,4-diacetyl oxazoline-5-one derivatives is shown in scheme 2. The initial activation of acetic anhydride is carried out by the catalyst. Then, the nucleophilic attack of hippuric acid on catalyst-activated acetic anhydride and subsequent elimination of acetate ion, cyclic intermediate (I) is formed. This intermediate, by loss of proton and tautomerization gives 2-phenyloxazol-5-ol (II), which immediately reacts with the aldehyde to give the desired product.

Also, the synthesis of 4-thiazolidinone derivatives through three-component reactions of aromatic aldehydes, anilines, and thioglycolic acid, in the presence of $ZnFe_2O_4$-TGA as an environmentally friendly green catalyst, was investigated. To find out the optimal reaction conditions, synthesis of 6a was selected as a model reaction. As summarized in Table 3 various solvents and different amounts of catalyst were investigated under different conditions. The best conditions for carrying out the

Table 3. The optimization of reaction conditions for synthesis of 3a as an oxazolone derivatives.

Entry	Solvent	Condition	Cat. (mg)	Time (min)	Yeild(%)[a]
1	THF	Reflux	20	120	55
2	$EtOCOCH_3$	Reflux	20	120	50
3	1,4-Dioxane	Reflux	20	120	40
4	$CHCl_3$	Reflux	20	120	5
5	CH_3CN	Reflux	20	120	55
6	-	25 °C	20	30	30
7	-	60 °C	20	30	45
8	-	90 °C	20	30	85
9	-	90 °C	-	30	-
10	-	MW	20	1	98
11	-	MW	10	1	84
12	-	MW	50	1	96
13	-	MW	-	1	-
14	-	MW	20	2	65

[a]Isolated yield. Model reaction: (benzaldehyde (1 mmol, 1 mL), hippuric acid (1 mmol, 0.165 g), and acetic anhydride (5 mmol, 0.5 g).

Table 4. The synthesis of oxazolone derivatives using ZnFe2O4 as a catalyst.

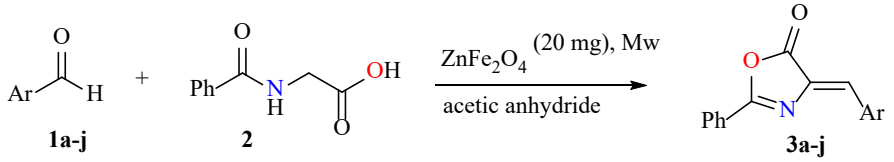

Entry	Ar	Time (min)	Yield (%)[a]	Azlactone	M.p (°C) [Lit]	
1	C_6H_5-	1	95	3a	170-172	168-170 [32]
2	4-MeC_6H_4-	1	90	3b	139-141	146-148 [33]
3	4-MeOC_6H_4-	1.5	95	3c	160-162	158-157 [34]
4	4-ClC_6H_4-	1	96	3d	201-203	205-206 [2]
5	4-$NO_2C_6H_4$-	1	94	3e	222-224	237-239 [35]
6	4-$(Me)_2NC_6H_4$-	1	98	3f	218-220	210-212 [36]
7	3-$NO_2C_6H_4$-	1	96	3g	172-174	166-168 [37]
8	2-C_4H_3S-	1	94	3h	181-183	178-179 [38]
9	2-MeOC_6H_4-	1.5	93	3i	170-172	155-156 [19]
10	4-FC_6H_4-	1	94	3j	188-190	185-183 [32]

[a] isolated yield. Condition: (aldehyde (1 mmol), hippuric acid (1 mmol, 0.165 g), and acetic anhydride (5 mmol, 0.5 g) in the presence of $ZnFe_2O_4$ (20 mg) as a catalyst microwave condition.

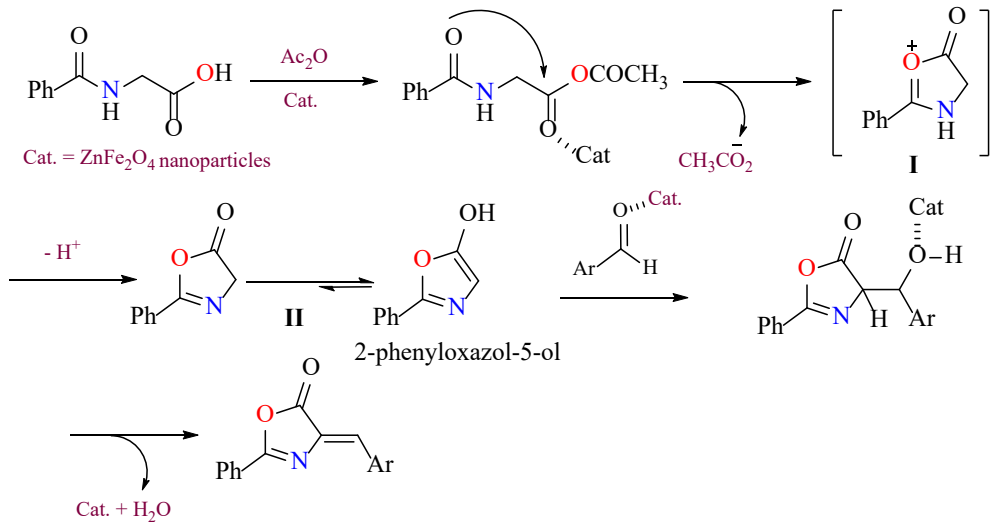

Scheme 2. The possible mechanism for the synthesis of oxazoline-5-one derivatives catalyzed by $ZnFe_2O_4$ nanoparticles.

reaction include 30 mg of catalyst, a temperature of 80 °C, and no use of solvent (Table 5).

After optimizing the conditions, the reaction was carried out with condensation of aniline (and paratoluidene), thioglycolic acid, and various aromatic aldehydes containing electron-donating and electron-withdrawing groups, and the results obtained are reported in Table 6.

The observed electron effects were such that electron-donating aromatic aldehydes needed

longer times to complete the reaction, and aromatic aldehydes with electron-withdrawing groups produced higher yields in shorter times. In addition, the catalytic activity of $ZnFe_2O_4$ MNPs and $ZnFe_2O_4$-TGA MNPs was compared with the results of other reported works (Table 7). As can be seen, the present study offers a new method with suitable catalytic activity for synthesis of oxazolone and 4-thiazolidinone derivatives.

A possible reaction mechanism for condensation of aniline, thioglycolic acid and benzaldehyde in the presence of zinc ferrite nanoparticles functionalized with thioglycolic acid is shown in scheme 3. Firstly, the carbonyl of aldehyde is activated by the Lewis acid cites of $ZnFe_2O_4$-TGA MNPs. Then the nucleophilic attack of aniline on the activated carbonyl group of aldehyde gives intermediate (I) after removal of H_2O. Subsequently, nucleophilic attack of the -SH group of thioglycolic acid on intermediate (I) produces intermediate (II), which upon elimination of water, leads to the formation of the desired product [49].

Table 5. Optimization of reaction conditions for synthesis of 6a as a 4-thiazolidinone derivatives.

Entry	Solvent	Condition	Cat. (mg)	Time (h)	Yield (%)[a]
1	Toluene	Reflux	30	12	60
2	CH_2Cl_2	Reflux	30	12	69
3	EtOH	Reflux	30	12	38
4	THF	Reflux	30	12	45
5	DMF	Reflux	30	12	56
6	H_2O	Reflux	30	12	33
7	-	30 °C	30	5	66
8	-	50 °C	30	1	82
9	-	80 °C	30	1	89
10	-	80 °C	30	1	70
11	-	80 °C	10	2	84
12	-	100 °C	30	1	75

[a] isolated yield.

Table 6. The synthesis of 4-thiazolidinone derivatives using $ZnFe_2O_4$-TGA MNPs as a catalyst.

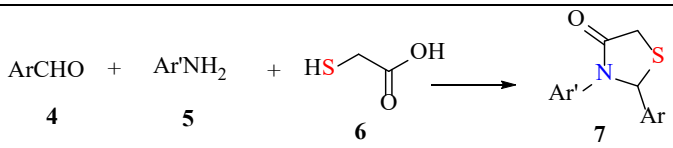

4 **5** **6** **7**

Entry	Ar'	Ar''	Time (h)	Yield (%)b	4-thiazolidinone	M.p (°C)	[Lit]Ref.
1	C_6H_5-	4-$CH_3C_6H_4$-	1	94	7a	105-107	106-107 [40]
2	4-ClC_6H_4	4-$CH_3C_6H_4$-	1	91	7b	154-158	162-164 [41]
3	3-$NO_2C_6H_4$-	4-$CH_3C_6H_4$-	1	87	7c	146-150	151-152 [42]
4	4-OHC_6H_4	4-$CH_3C_6H_4$-	1	80	7d	153-158	127-129 [43]
5	3-$NO_2C_6H_4$-	4-BrC_6H_4-	1	77	7e	160-163	-
6	3-$NO_2C_6H_4$-	3,4,5-ClC_6H_2-	1	70	7f	164-166	-

3.3. Catalyst recovery and reusability

The reusability of both $ZnFe_2O_4$ and $ZnFe_2O_4$-TGA nanocatalysts was investigated under specific reaction conditions. At first, benzaldehyde (1 mmol), hippuric acid (1 mmol), and acetic anhydride (0.5 g) were combined with $ZnFe_2O_4$, followed by magnetic separation of the catalyst after reaction completion. Subsequent washing with ethanol and double distilled water ensured catalyst purification. As depicted in Figure 7a 7b, the recovered catalyst retained its activity remarkably well over five cycles (95% to 92%), demonstrating excellent reusability.

Table 7. The comparison of catalytic activity of ZnFe2O4 MNPs and ZnFe2O4-TGA MNPs with other reported works for 3a and 7a.

	Entry	catalyst	conditions	Yield%	Reference
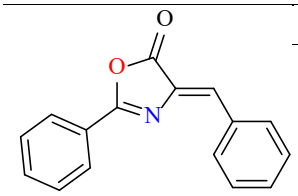 3a	1	$(CH_3CO)_2O/CH_3COONa$	Reflux, 3h	72	[44]
	2	$(CH_3CO)_2O/CH_3COONa$	Grinding, solvent free, r.t 4-13 min	90	[45]
	3	$(CH_3CO)_2O/PPh_3$	Solvent free, 18 min, 130°C	94	[39]
	4	$ZnFe_2O_4/(CH_3CO)_2O$	microwave power (450W), 1 min	95	This work
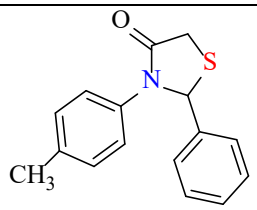 7a	5	$[Et_3NH][HSO_4]$	solvent free, 80°C, 30 min	94	[46]
	6	MNP@SiO_2-IL	solvent free, 70°C, 60 min	90	[47]
	7	$FeNi_3$-IL MNPs	Solvent free, 50°C	90	[48]
	8	$ZnFe_2O_4$-TGA	solvent free, 80°C, 1h	89	This work

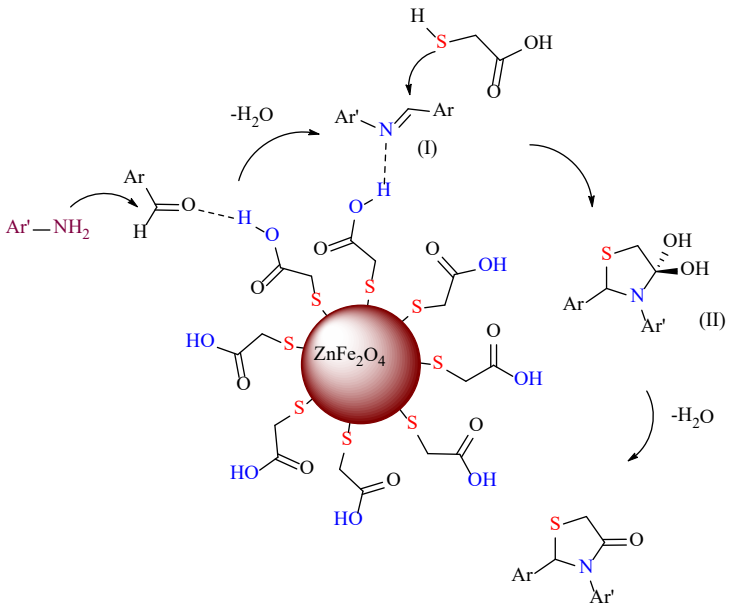

Scheme 3. The proposed mechanism for the synthesis of 4-thiazolidinone derivatives (1,3-thiazolidine-4-one) in the presence of zinc ferrite nanoparticles functionalized with thioglycolic acid.

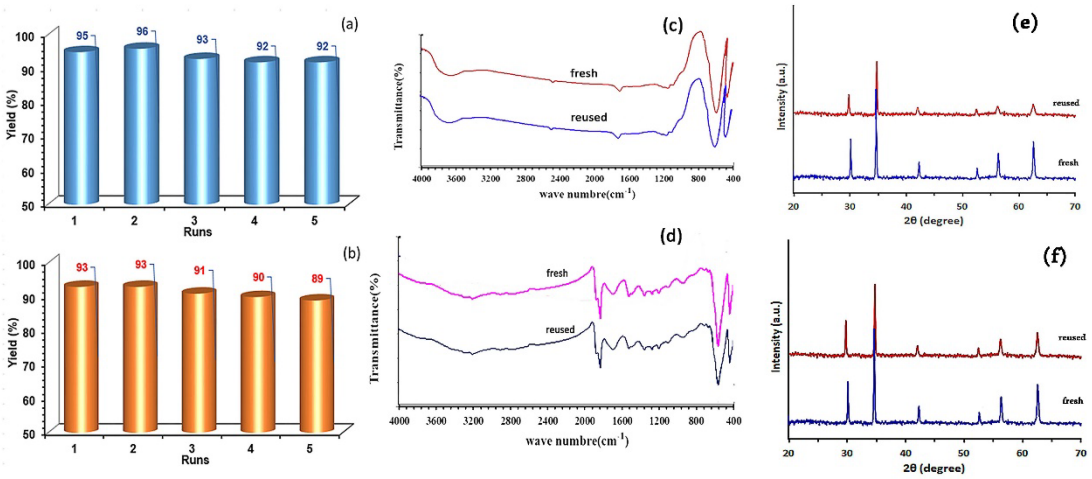

Fig. 7. Recyclability of (a) ZnFe2O4 and (b) ZnFe2O4-TGA, FT-IR spectra of fresh and reused of ZnFe2O4 (c), and ZnFe2O4-TGA (d), XRD patterns of reused and fresh, ZnFe2O4 (e), and ZnFe2O4-TGA (f),

Similarly, the reusability of $ZnFe_2O_4$-TGA was assessed using benzaldehyde (1 mmol), para-toluidine (1 mmol), and thioglycolic acid (1.5 mmol) in the presence of the nanocatalyst. After magnetic separation and sequential washing with tetrahydrofuran and double distilled water, the catalyst exhibited consistent activity across five cycles (93% to 89%) (Figure 7b).

Furthermore, the structural stability of the used catalysts was confirmed through FT-IR and XRD analyses. Comparison of the FT-IR spectra (Figures 7c and 7d) and XRD patterns of the fresh and post-reaction catalysts (Figures 7e and 7f) showed no significant changes, indicating a remarkable structural integrity even after several cycles of use.

4. Conclusions

In this study, zinc ferrite ($ZnFe_2O_4$) and zinc ferrite functionalized thioglycolic acid ($ZnFe_2O_4$-TGA) nanoparticles were successfully synthesized through a green, cost-effective, and simple approach using walnut leaves. To investigate the catalytic activity of $ZnFe_2O_4$ and $ZnFe_2O_4$-TGA nanoparticles, their effectiveness in the synthesis of oxazolone and thiazolidinedione derivatives was investigated. Short reaction times, high product yields, and easy workup are among the advantages of this method in the presence of the desired green and reusable catalysts.

Both $ZnFe_2O_4$ and $ZnFe_2O_4$-TGA nanoparticles exhibit remarkable stability and retain their catalytic activity over multiple reaction cycles. Overall, this study highlights the potential of environmentally friendly magnetic nanocatalysts in the synthesis of valuable heterocyclic compounds and takes an important step towards environmentally friendly chemical processes.

Acknowledgements

We gratefully acknowledge the financial support of this work by the research council of Arak University.

Conflicts of Interest

The authors declare that they have no known competing financial interests or personal relationships that could have appeared to influence the work reported in this paper.

References

[1] S. Thakur, A. Bhalla, Sustainable synthetic endeavors of pharmaceutically active Schiff bases and their metal complexes: A review on recent reports, Tetrahedron 153 (2024) 133836. https://doi.org/10.1016/j.tet.2024.133836

[2] M. Kalhor, M. Bigdeli, H. Moghanian, Ni@zeolite-Fe_3O_4 supported 4-methylpyridinium ionic liquid: design and application as a new multi-functional and magnetically catalytic nanosystem in three-component synthesis of 4-aryl oxazolones, Res. Chem. Intermed. 49(12) (2023) 5375-5394.https://doi.org/10.1007/s11164-023-05146-9

[3] R.K. Sindhu, K. Rani, V. Singh, Y. Singh, B. Hans, M.A. Babu, A. Goyal, Basics of Nanotechnology and Drug Delivery Systems, Nanotechnology and Drug Delivery, Jenny Stanford Publishing2024, pp. 1-59.

[4] F. Wang, X. Wang, X. Lu, C. Huang, Nanophotonic enhanced chiral sensing and its biomedical applications, Biosensors 14(1) (2024) 39. https://doi.org/10.3390/bios14010039

[5] L. Li, T. Wang, Y. Zhong, R. Li, W. Deng, X. Xiao, Y. Xu, J. Zhang, X. Hu, Y. Wang, A review of nanomaterials for biosensing applications, J. Mater. Chem. B 12(5) (2024) 1168-1193. https://doi.org/10.1039/D3TB02648E

[6] J. Sharma, P. Kumar, M. Sillanpaa, D. Kumar, M. Nemiwal, Immobilized ionic liquids on Fe_3O_4 nanoparticles: A potential catalyst for organic synthesis, Inorg. Chem. Commun. 145 (2022) 110055. https://doi.org/10.2139/ssrn.4119246

[7] S.H. Gebre, Recent developments of supported and magnetic nanocatalysts for organic transformations: an up-to-date review, Appl. Nanosci. 13(1) (2023) 15-63. https://doi.org/10.1007/s13204-021-01888-3

[8] P. Rai, D. Gupta, Magnetic nanoparticles as green catalysts in organic synthesis-a review, Synth. Commun. 51(20) (2021) 3059-3083. https://doi.org/10.1080/00397911.2021.1968910

[9] M. Kurian, S. Thankachan, Structural diversity and applications of spinel ferrite core-Shell nanostructures-A review, Open Ceram. 8 (2021) 100179. https://doi.org/10.1016/j.oceram.2021.100179

[10] A. Goyal, S. Bansal, S. Singhal, Facile reduction of nitrophenols: Comparative catalytic efficiency of MFe_2O_4 (M= Ni, Cu, Zn) nano ferrites, International journal of hydrogen energy 39(10) (2014) 4895-4908. https://doi.org/10.1016/j.ijhydene.2014.01.050

[11] S. Iravani, Green synthesis of metal nanoparticles using plants, Green Chem. 13(10) (2011) 2638-2650. https://doi.org/10.1039/C1GC15386B

[12] T. Đorđević, R. Đurović-Pejčev, M. Stevanović, M. Sarić-Krsmanović, L. Radivojević, L. Šantrić, J. Gajić-Umiljendić, Phytotoxicity and allelopathic potential of Juglans regia L. leaf extract, Frontiers in Plant Science 13 (2022) 986740

[13] H. Korbekandi, G. Asghari, S.S. Jalayer, M.S. Jalayer, M. Bandegani, Nanosilver particle production using Juglans Regia L.(walnut) leaf extract, Jundishapur Journal of Natural Pharmaceutical Products 8(1) (2013) 20

[14] L. Kumar, K. Lal, A. Kumar, A. Kumar, Synthesis, antimicrobial evaluation and docking studies of oxazolone-1, 2, 3-triazole-amide hybrids, Res. Chem. Intermed. 47(12) (2021) 5079-5097. https://doi.org/10.1007/s11164-021-04588-3

[15] H.-Z. Zhang, Z.-L. Zhao, C.-H. Zhou, Recent advance in oxazole-based medicinal chemistry, Eur. J. Med. Chem. 144 (2018) 444-492. https://doi.org/10.1016/j.ejmech.2017.12.044

[16] D.S. Haneen, W.S. Abou-Elmagd, A.S. Youssef, 5 (4 H)-oxazolones: synthesis and biological activities, Synth. Commun. 51(2) (2021) 215-233. https://doi.org/10.1080/00397911.2020.1825746

[17] A. Scala, A. Piperno, N. Micale, F. Christ, Z. Debyser, Synthesis and anti-HIV profile of a novel tetrahydroindazolylbenzamide derivative obtained by oxazolone chemistry, ACS Med. Chem. Lett. 10(4) (2018) 398-401. https://doi.org/10.1021/acsmedchemlett.8b00511

[18] S.A. Jadhav, A.P. Sarkate, M. Farooqui, D.B. Shinde, Greener approach: Ionic liquid $[Et_3NH][HSO_4]$-catalyzed multicomponent synthesis of 4-arylidene-2-phenyl-5 (4 H) oxazolones under solvent-free condition, Synth. Commun. 47(18) (2017) 1676-1683. https://doi.org/10.1080/00397911.2017.1340649

[19] H. Moghanian, M. Shabanian, H. Jafari, Microwave-assisted efficient synthesis of azlactone derivatives using TsCl/DMF under solvent-free conditions, C.R. Chim. 15(4) (2012) 346-349. https://doi.org/10.1016/j.crci.2011.11.011

[20] M.R. Buemi, R. Gitto, L. Ielo, C. Pannecouque, L. De Luca, Inhibition of HIV-1 RT activity by a new series of 3-(1, 3, 4-thiadiazol-2-yl) thiazolidin-4-one derivatives, Bioorg. Med. Chem. 28(8) (2020) 115431. https://doi.org/10.1016/j.bmc.2020.115431

[21] S. Tummalacharla, P. Padmaja, P.N. Reddy, An efficient one-pot synthesis of pyrazolyl-2-thioxothiazolidin-4-one hybrid analogues and evaluation of their antimicrobial activity, Chem. Data Collect. 31 (2021) 100600. https://doi.org/10.1016/j.cdc.2020.100600

[22] B. Qi, X. Xu, Y. Yang, Y. Zhou, T. Chen, G. Gong, X. Yue, X. Xu, L. Hu, H. He, Discovery of thiazolidin-4-one urea analogues as novel multikinase inhibitors that potently inhibit FLT3 and VEGFR2, Bioorg. Med. Chem. 27(10) (2019) 2127-2139. https://doi.org/10.1016/j.bmc.2019.03.049

[23] R. Hajiarab, M.R.M. Shafiee, M. Ghashang, Preparation of thiazolidin-4-ones using $NiFe_2O_4$@SiO_2 grafted propylsulfonic acid as an efficient catalyst, Org. Prep. Proced. Int. 54(3) (2022) 259-267. https://doi.org/10.1080/00304948.2022.2033064

[24] K.M. Gokhale, V.N. Telvekar, Silica chloride (SiO_2-Cl) catalyzed one pot synthesis of 2, 3-disubstituted-thiazolidin-4-one, Synth. Commun. 50(9) (2020) 1396-1403. https://doi.org/10.1080/00397911.2020.1741641

[25] D.D. Andhare, S.R. Patade, J.S. Kounsalye, K. Jadhav, Effect of Zn doping on structural, magnetic and optical properties of cobalt ferrite nanoparticles synthesized via. Co-precipitation method, Physica B 583 (2020) 412051. https://doi.org/10.1016/j.physb.2020.412051

[26] A.R. Abbasian, M. Shafiee Afarani, One-step solution combustion synthesis and characterization of $ZnFe_2O_4$ and $ZnFe_{1.6}O_4$ nanoparticles, Appl. Phys. A 125(10) (2019) 721. https://doi.org/10.1007/s00339-019-3017-7

[27] D. Maiti, A. Saha, P.S. Devi, Surface modified multifunctional $ZnFe_2O_4$ nanoparticles for hydrophobic and hydrophilic anti-cancer drug molecule loading, Phys. Chem. Chem. Phys. 18(3) (2016) 1439-1450. https://doi.org/10.1039/C5CP05840F

[28] M. Shafiee, S. Hafez Ghoran, S. Bordbar, M. Gholami, M. Naderian, F.S. Dehghani, A.M. Amani, Rutin: a flavonoid precursor for synthesis of ZnFe2O4 nanoparticles; electrochemical study of zinc ferrite-chitosan nanogel for doxorubicin delivery, J. Nanostruct. 11(1) (2021) 114-124. https://doi.org/10.22052/JNS.2021.01.013

[29] N. Biglari, A. Nasiri, S. Pakdel, M. Nasiri, Facile and reliable route for synthesis of zinc ferrite nanoparticles and its application in photo-degradation of methyl orange, J Mate Scienc: Mater Electron 27(12) (2016) 13113-13118

[30] D.J. Patil, S.N. Behera, Synthesizing nanoparticles of zinc and copper ferrites and examining their potential to remove various organic dyes through comparative studies of kinetics, isotherms, and thermodynamics, Environmental Monitoring and Assessment 195(5) (2023) 591. https://doi.org/10.1007/s10661-023-11177-x

[31] N.S. Mirani, F. Ghayem, S. Hosseini, S.A. Pourmousavi, ZnFe2O4@ Fe3O4 nanocatalyst for the synthesis of the 1, 8-dioxooctahydroxanthene: antioxidant and antimicrobial studies, (2023)

[32] N.C. Desai, A.S. Maheta, A.M. Jethawa, U.P. Pandit, I. Ahmad, H. Patel, Zeolite (Y-H)-based green synthesis, antimicrobial activity, and molecular docking studies of imidazole bearing oxydibenzene hybrid molecules, J. Heterocycl. Chem. 59(5) (2022) 879-889. https://doi.org/10.1002/jhet.4427

[33] A.M.L. Punna Rao, A. Sridhar Rao, M. Saratchandra Babu, M. Krishnaji Rao, Triphenylphosphine (PPh_3) Catalyzed Erlenmeyer Reaction for Azlactones under Solvent-free Conditions, J. Heterocycl. Chem. 54(1) (2017) 429-435. https://doi.org/10.1002/jhet.2600

[34] P.A. Conway, K. Devine, F. Paradisi, A simple and efficient method for the synthesis of Erlenmeyer azlactones, Tetrahedron 65(15) (2009) 2935-2938. https://doi.org/10.1002/chin.200933133

[35] N. Rostamizadeh, A. Khajeh-Amiri, H. Moghanian, Microwave-assisted Erlenmeyer synthesis of azlactones catalyzed by MgO/Al_2O_3 under solvent-free conditions, Synth. React. Inorg. Met. Org. Chem. 46(5) (2016) 631-634. https://doi.org/10.1080/15533174.2014.989575

[36] C.I. Esteves, I. da Silva Fonseca, J. Rocha, A.M. Silva, S. Guieu, Synthesis and luminescence properties of analogues of the green fluorescent protein chromophore, Dyes Pigm. 177 (2020) 108267. https://doi.org/10.1016/j.dyepig.2020.108267

[37] B.R. Madje, M.B. Ubale, J.V. Bharad, M.S. Shingare, Alum an efficient catalyst for Erlenmeyer synthesis : research article, S. Afr. J. Chem. 63(1) (2010) 158-161. https://doi.org/10.10520/EJC24503

[38] A.M. Tikdari, S. Fozooni, H. Hamidian, Dodecatungstophosphoric acid ($H_3PW_{12}O_{40}$), samarium and ruthenium (III) chloride catalyzed synthesis of unsaturated 2-phenyl-5 (4H)-oxazolone derivatives under solvent-free conditions, Molecules 13(12) (2008) 3246-3252. https://doi.org/10.3390/molecules13123246

[39] A.M.L. Punna Rao, A. Sridhar Rao, M. Saratchandra Babu, M. Krishnaji Rao, Triphenylphosphine (PPh3) Catalyzed Erlenmeyer Reaction for Azlactones under Solvent-free Conditions, Journal of Heterocyclic Chemistry 54(1) (2017) 429-435. https://doi.org/10.1002/jhet.2600

[40] S.P. Gadekar, M.K. Lande, TS-1 zeolite as a Lewis acid catalyst for solvent-free one-pot synthesis of 1, 3-thiazolidin-4-ones, Res. Chem. Intermed. 45(2) (2019). https://doi.org/10.1007/s11164-018-3599-2

[41] D.D. Subhedar, M.H. Shaikh, M.A. Arkile, A. Yeware, D. Sarkar, B.B. Shingate, Facile synthesis of 1, 3-thiazolidin-4-ones as antitubercular agents, Bioorg. Med. Chem. Lett. 26(7) (2016) 1704-1708. https://doi.org/10.1016/j.bmcl.2016.02.056

[42] N. Foroughifar, S. Ebrahimi, One-pot synthesis of 1, 3-thiazolidin-4-one using $Bi(SCH_2COOH)_3$ as catalyst, Chin. Chem. Lett. 24(5) (2013) 389-391. https://doi.org/10.1016/j.cclet.2013.03.019

[43] H. Taghrir, M. Ghashang, Preparation of 2, 3-diarylthiazolidin-4-one derivatives using barium molybdate nanopowders, Synth. React. Inorg. Met. Org. Chem. 46(2) (2016) 246-250. https://doi.org/10.1080/15533174.2014.988227

[44] L. Jat, R. Mishra, D. Pathak, Synthesis and anticancer activity of 4-Benzylidene-2-phenyloxazol-5 (4H)-one derivatives, Int J Pharm Pharm Sci 4(1) (2012) 378-380. https://doi.org/10.33263/BRIAC111.80968109

[45] A.F. Fahmy, A.A. El-Sayed, M.M. Hemdan, Multicomponent synthesis of 4-arylidene-2-phenyl-5 (4H)-oxazolones (azlactones) using a mechanochemical approach, Chem Centr J 10(1) (2016) 59. https://doi.org/10.1186/s13065-016-0205-9

[46] D.D. Subhedar, M.H. Shaikh, M.A. Arkile, A. Yeware, D. Sarkar, B.B. Shingate, Facile synthesis of 1, 3-thiazolidin-4-ones as antitubercular agents, Bioorg. Med. Chem. Lett 26(7) (2016) 1704-1708. https://doi.org/10.1016/j.bmcl.2016.02.056

[47] N. Azgomi, M. Mokhtary, Nano-Fe3O4@ SiO2 supported ionic liquid as an efficient catalyst for the synthesis of 1, 3-thiazolidin-4-ones under solvent-free conditions, J. Mole. Catal A: Chemical 398 (2015) 58-64. https://doi.org/10.1016/j.molcata.2014.11.018

[48] S.M. Sadeghzadeh, F. Daneshfar, Ionic liquid immobilized on FeNi3 as catalysts for efficient, green, and one-pot synthesis of 1, 3-thiazolidin-4-one, J. Mole. Liq. 199 (2014) 440-444. https://doi.org/10.1016/j.molliq.2014.07.039

[49] S.P. Gadekar, M.K. Lande, TS-1 zeolite as a Lewis acid catalyst for solvent-free one-pot synthesis of 1, 3-thiazolidin-4-ones, Res. Chem. Intermed 45 (2019) 237-247. https://doi.org/10.1007/s11164-018-3599-2